

Black Si Photocathode with a Conformal and Amorphous MoS_x Catalytic Layer Grown Using Atomic Layer Deposition for Photoelectrochemical Hydrogen Evolution

Dae Woong Kim,[#] Jin-Young Jung,[#] Dae Hyun Kim, Jin-Young Yu, Jae Hyuck Jang, Hyun Soo Jin, Tae Jun Seok, Yo-Sep Min,^{*} Jung-Ho Lee,^{*} and Tae Joo Park^{*}



Cite This: *ACS Appl. Mater. Interfaces* 2022, 14, 14137–14145



Read Online

ACCESS |



Metrics & More



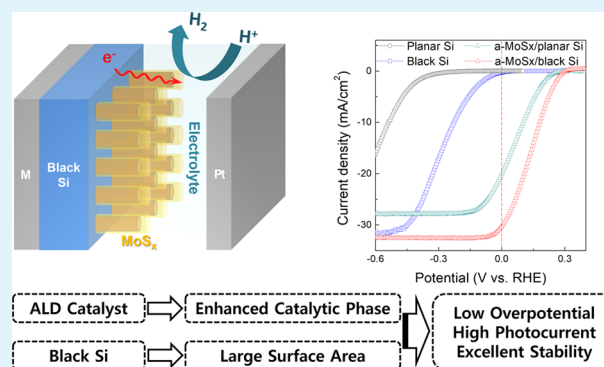
Article Recommendations



Supporting Information

ABSTRACT: We demonstrated how the photoelectrochemical (PEC) performance was enhanced by conformal deposition of an amorphous molybdenum sulfide (a-MoS_x) thin film on a nanostructured surface of black Si using atomic layer deposition (ALD). The a-MoS_x is found to predominantly consist of an octahedral structure (S-deficient metallic phase) that exhibits high electrocatalytic activity for the hydrogen evolution reaction with a Tafel slope of 41 mV/dec in an acid electrolyte. The a-MoS_x has a smaller work function (4.0 eV) than that of crystalline 2H-MoS₂ (4.5 eV), which induces larger energy band bending at the p-Si surface, thereby facilitating interface charge transfer. These features enabled us to achieve an outstanding kinetic overpotential of ~0.2 V at 10 mA/cm² and an onset potential of 0.27 V at 1 mA/cm². Furthermore, the a-MoS_x layer provides superior protection against corrosion of the Si surface, enabling long-term PEC operation of more than 50 h while maintaining 87% or more performance. This work highlights the remarkable advantages of the ALD a-MoS_x layer and leads to a breakthrough in the architectural design of PEC cells to ensure both high performance and stability.

KEYWORDS: photoelectrochemical cell, hydrogen evolution, black Si, amorphous MoS_x, atomic layer deposition



INTRODUCTION

Photoelectrochemical (PEC) cells, which drive water splitting reactions through light-induced charge carriers at semiconductor photoelectrodes, are ideal for economically generating clean and sustainable hydrogen fuel.¹ Among various semiconductor materials, silicon is a low-cost and earth-abundant material with a narrow band gap (1.12 eV) capable of absorbing incident light over a wide range of wavelengths, including light in the visible and near-infrared (NIR) regions. In particular, a nanostructured surface of black Si is considered a promising architecture to achieve high PEC performance because of its excellent antireflection capability, which can minimize light reflectance and generate a high photocurrent level. In addition, acting as an efficient architecture strategy, the large active area of the nanostructured surface can facilitate interface charge transfer for PEC reactions,^{2–7} and the short travel distance of the charge carriers along the nanostructure diameter can effectively improve the carrier collection efficiency.⁵ Despite these benefits, the complex surface morphology of black Si makes it difficult to form functional building blocks on it, such as an electrocatalyst, emitter, or protective layer. However, conformal deposition of a continuous thin film that can protect the

nanostructured surface from corrosive electrolytes is essential to ensure long-term, stable PEC reactions.

One of the best techniques to deposit a conformal, continuous thin film on a nanostructure surface is the atomic layer deposition (ALD) process, which can grow high-quality thin films with excellent step coverage. Typically, ALD TiO_x thin films, which have high corrosion resistance to a range of electrolyte pHs and sufficiently high atomic density to prevent electrolyte permeation, are incorporated as a protection layer. The incorporated TiO_x layer greatly improves the stability, but it inevitably causes additional electrical resistance that degrades the PEC performance in proportion to its thickness.⁸ One way to minimize the interfacial resistance is to employ a conformal thin film that simultaneously serves as an electrocatalyst and a protection layer. For example, it has been reported that CoO_x thin films made using ALD to form an n-Si photoanode with a

Received: November 16, 2021

Accepted: March 3, 2022

Published: March 15, 2022



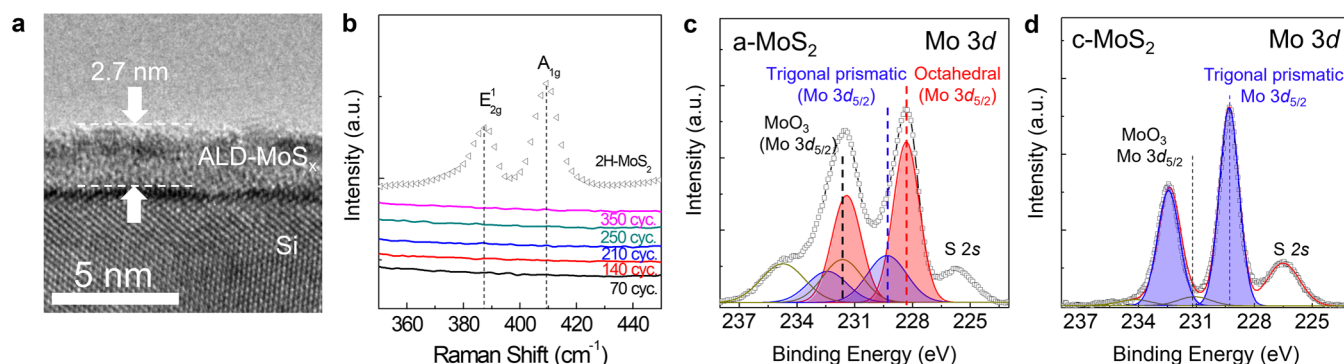


Figure 1. (a) Cross-sectional HR-TEM image of ALD a-MoS_x film grown with 70 cycles on an Si substrate. (b) Raman spectroscopy results for ALD a-MoS_x films with various thicknesses and c-MoS₂ film confirming the amorphous nature of the a-MoS_x film. Mo 3d core-level spectra with deconvolution results of (c) a-MoS_x and (d) c-MoS₂ films on Si substrates suggesting that the a-MoS_x and c-MoS₂ films are mostly composed of the electrocatalytically active amorphous phase and 2H-MoS₂ phase, respectively.

slightly rough surface for the oxygen evolution reaction (OER) ensured both electrocatalytic activity and stability.⁹

To ensure an efficient hydrogen evolution reaction (HER), noble metal-based electrocatalysts, such as Pt, Ru, and Ir, which exhibit the best electrocatalytic activity, are generally used. However, these are relatively expensive, scarce, and difficult to deposit evenly on the surface of nanostructures, limiting their widespread use for PEC devices.^{10,11} Recently, earth-abundant MoS₂ has attracted attention as a promising alternative, exhibiting excellent HER electrocatalytic activity in both crystalline and amorphous structures.^{12–18} For crystalline MoS₂ (c-MoS₂), the edge sites are more electrocatalytically active than the basal planes because the hydrogen adsorption free energy for the HER is much lower on the edge sites.^{19–22} Several approaches have been proposed to enlarge the number of active sites (and active area) and enhance the catalytic activity. The defect density on the mainly exposed basal plane can be increased by doping other elements such as Se and Cl and generating S vacancies or strain, which exposes more of the active Mo inner layers.^{20,23} Morphological engineering such as the growth of vertically aligned three-dimensional structures and stacked two-dimensional layers has also been exploited to expose more active edge sites.^{24,25} Interestingly, the phase transition of thermodynamically stable 2H-MoS₂ into metastable 1T-MoS₂ was also reported as an effective way to improve the activity.^{12,16,26} The 1T-MoS₂ synthesized by low-temperature growth or exfoliation by Li intercalation has a metallic nature and lots of catalytic active sites compared to 2H-MoS₂. Recent studies by Merki et al., Lu et al., and Vrabel et al. revealed that amorphous MoS_x (a-MoS_x) thin films have an inherently active phase with an S deficiency and exposure of the inner Mo layer.^{19–22} This material exhibited comparable electrocatalytic activity to that of the most active c-MoS₂.^{19–22}

In this work, a-MoS_x ($x = 1.7$) thin films were grown on Si photocathodes as the electrocatalytic layer using a wafer-scale ALD process at a low temperature (<200 °C) while alternately supplying Mo(CO)₆ and H₂S precursors. The a-MoS_x mostly has an octahedral Mo–S binding structure (S-deficient metallic phase), which leads to high electrocatalytic activity for the HER in an H₂SO₄ electrolyte. In addition, the lower work function of a-MoS_x (4.0 eV) compared to that of the typical crystalline MoS₂ (4.5 eV) developed larger band bending at the a-MoS_x/Si junction. We found that the optimal thickness (~3.5 nm) maximized both the electrocatalytic activity and Si surface band bending; this is the critical thickness needed to

make a continuous thin film. As a result, a low kinetic overpotential and high onset potential (V_{on}) for the PEC reaction were achieved with the a-MoS_x/Si photocathode; these values are superior to values in the literature for 2H-MoS₂/Si photocathodes. Moreover, coating a conformal ALD a-MoS_x layer on the black Si photocathode further decreased the overpotential by enlarging the active area while also ensuring excellent protection, thereby enabling great improvements in the PEC performance and long-term stability.

RESULTS AND DISCUSSION

Figure 1a shows a high-resolution transmission electron microscopy (HRTEM) image of a 2.7 nm-thick continuous MoS_x thin film (70 cycles) grown using ALD on a flat Si substrate.²⁷ The linear increase in the thickness of the MoS_x layer with an increasing number of ALD cycles confirmed the ALD reaction and growth (Figure S1). A relatively low growth temperature of 178 °C resulted in the a-MoS_x layer.²⁸ The Raman spectroscopy results in Figure 1b confirm the amorphous nature of the a-MoS_x films with various ALD cycles; these were compared to those of the c-MoS_x film (2H phase) crystallized by rapid thermal annealing (RTA). Raman spectroscopy is generally used to analyze the crystal structure of ultrathin transition metal dichalcogenides.^{29–31} The crystalline MoS_x film shows two prominent peaks of the in-plane E_{2g} mode at 385 cm^{−1} and the out-of-plane A_{1g} phonon mode at 409 cm^{−1}. However, no peak was observed for the a-MoS_x film. The chemical state of the a-MoS_x film was examined with X-ray photoelectron spectroscopy (XPS), as shown in Figure 1c, which shows the Mo 3d core-level spectrum with the deconvolution results. Three peaks are observed. The Mo 3d_{5/2} peaks at binding energies (BEs) of 228.4, 229.4, and 231.6 eV (red, blue, and black dashed lines, respectively) correspond to octahedral Mo^(IV) (metallic phase), trigonal prismatic Mo^(IV) (semiconducting 2H phase), and MoO₃, respectively.^{16,20,26,32,33} Therefore, the as-grown a-MoS_x film is mostly composed of the electrocatalytically active amorphous phase (locally metallic, octahedral structure). The atomic ratio of Mo/S is ~1:1.7, indicating that the film contains a considerable number of S vacancies (Figure S2).^{20,23} This ALD a-MoS_x containing an oxysulfide phase might deteriorate the HER catalytic properties through excessive Mo–O bond formation. However, Shin et al. reported that locally incorporated oxygen could positively affect the HER performance of a-MoS_x by increasing the intrinsic electrical

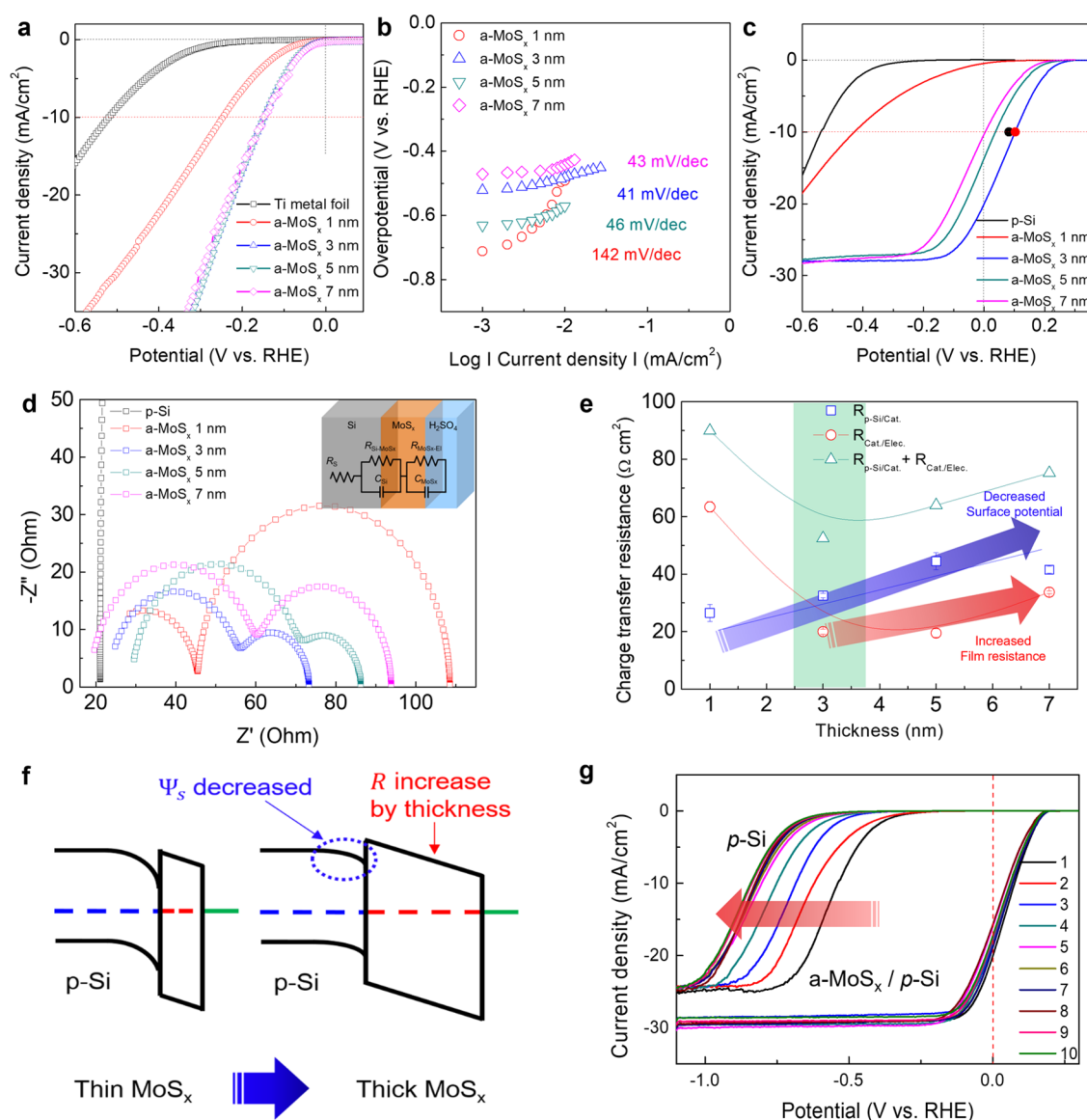


Figure 2. (a) LSV response curves of ALD a-MoS_x layers with various thicknesses grown on a Ti foil to estimate the HER electrocatalytic activity. (b) Tafel slopes of a-MoS_x layers on Ti foil based on the LSV curves. (c) LSV response curves and (d) EIS analysis results of ALD a-MoS_x films with various thicknesses grown on Si photocathodes, by which the thickness of a-MoS_x layers was optimized at 3 nm. (e) Charge transfer resistances calculated based on the EIS results as a function of the a-MoS_x thickness. (f) Schematic energy band diagrams of the a-MoS_x/Si structures with thin and thick MoS_x layers explaining the changes in the charge transfer resistance. (g) LSV curves with cyclic tests of bare Si and the a-MoS_x/Si photocathode, showing that the 3 nm-thick a-MoS_x layer significantly improved the stability of the photocathode.

conductivity and forming active sites.³⁴ In general, excessive O is a deterioration factor, but orthorhombic MoO₃ and 1T-MoS₂ share a similar octahedral crystal structure, so replacing S with O in an appropriate amount might form a metallic 1T phase. Crystalline 2H-MoS₂ shows only one doublet peak corresponding to the trigonal prismatic Mo^(IV), as shown in Figure 1d.

Linear sweep voltammetry (LSV) responses of a-MoS_x thin films of varying thicknesses grown on Ti foil were examined to identify the HER electrocatalytic activity of a-MoS_x films and to optimize the thickness, as shown in Figure 2a. The electrocatalytic activity was observed in a 0.5 M H₂SO₄ electrolyte based on an Ag/AgCl reference electrode. The growth of a-MoS_x shifts the LSV curves in the anodic direction, indicating a reduction in the kinetic overpotential required for charge transfer; this means that the HER electrocatalytic

activity was improved. The overpotential vs reversible hydrogen electrode (RHE) required at 10 mA/cm² was −0.245 V for 1 nm-thick a-MoS_x, which decreased to −0.153 V at a thickness of 3 nm and then saturated with further increases in the a-MoS_x thickness. This is because the ALD MoS_x layer with a nominal thickness of ~1 nm (in the initial growth stage) is not continuous due to its island growth nature, but the increase in thickness to ~3 nm leads to continuous film growth covering the entire Si surface (at 3 nm). This is consistent with the AFM results. The RMS roughness of the 1 nm-thick MoS_x layer was relatively high due to the MoS_x islands, and it decreased with increasing MoS_x thickness up to 3 nm because the coalescence of islands resulted in the formation of a continuous layer (Figure S3). Once the conformal MoS_x layer was formed, the HER electrocatalytic activity was improved and maintained when the thickness was increased further.

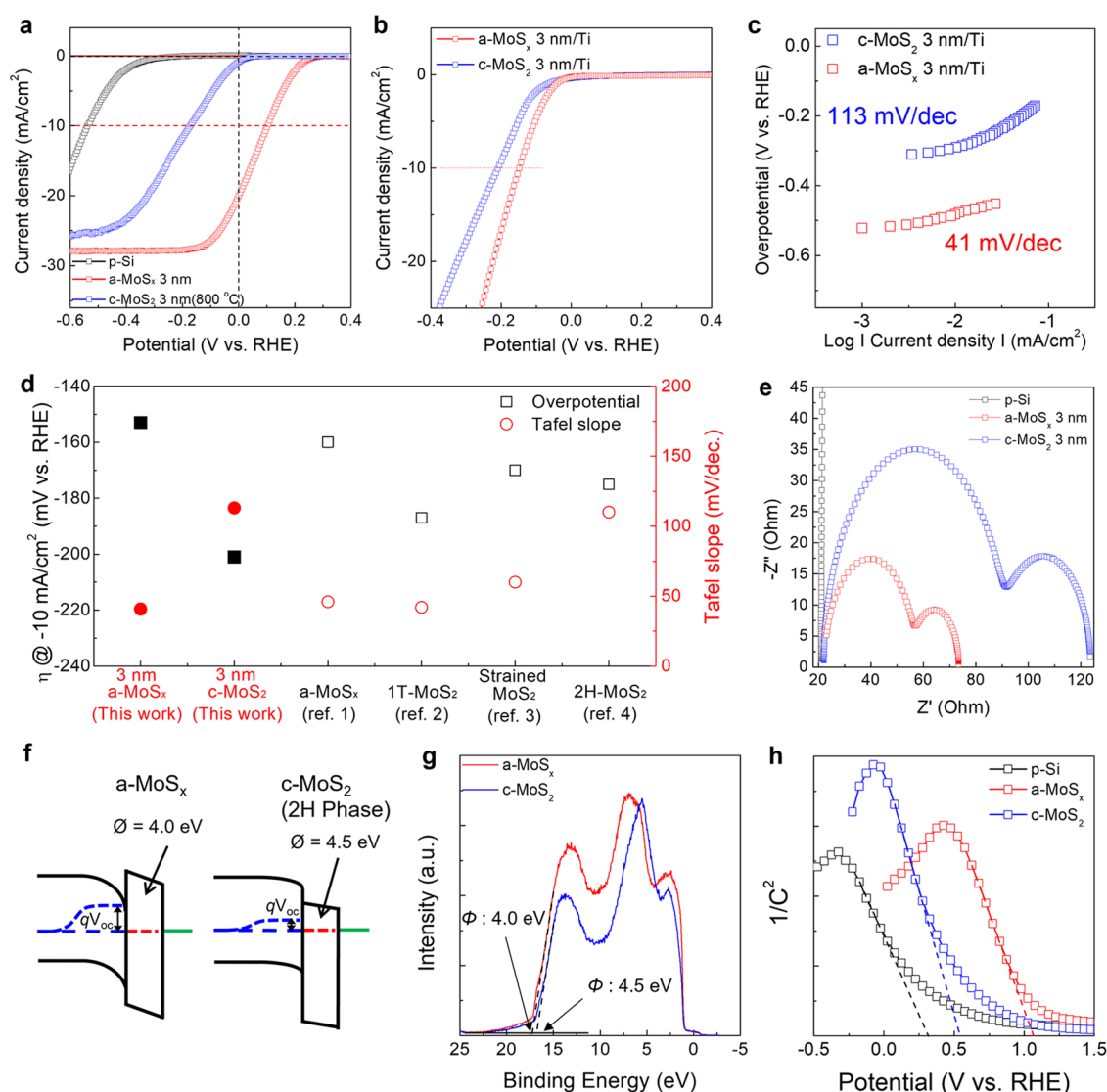


Figure 3. (a) LSV response curves of Si photocathodes with the a-MoS_x and c-MoS₂ layers, showing that the overpotential of the photocathode with the a-MoS_x layer is significantly improved compared to that with the c-MoS₂ layer. (b) LSV response curves of ALD a-MoS_x and c-MoS₂ layers on Ti foil to estimate HER electrocatalytic activity. (c) Tafel slope comparison of a-MoS_x and c-MoS₂ layers on Ti foil based on the LSV curves. (d) Overpotential and Tafel slopes for a-MoS_x and c-MoS₂ were summarized and compared to various reported values. (e) EIS analysis results, (f) schematic energy band diagrams, (g) UPS spectra for estimating the work function, and (h) Mott–Schottky plots (1/C² vs V) of Si photocathodes with the a-MoS_x and c-MoS₂ layers. The lower work function of the a-MoS_x layer induced higher Si surface band bending, which results in the lower charge transfer resistance.

The Tafel plots based on the LSV curves in Figure 2b identify the rate-determining step among the three reactions for the HER, which include the Volmer (>120 mV/dec), Heyrovsky (>40 mV/dec), and Tafel (<30 mV/dec) steps. This Tafel slope is indicative of the reaction steps in the HER, and a lower value is better. The first Volmer step is the proton discharge step ($\text{H}^+(\text{aq}) + \text{e}^- = \text{H}_{\text{ads}}^*$), which is followed by the Heyrovsky step with electrochemical desorption ($\text{H}_{\text{ads}}^* + \text{H}^+(\text{aq}) + \text{e}^- \rightarrow \text{H}_2 + *$) and the Tafel step with a chemical desorption reaction ($2\text{H}_{\text{ads}}^* \rightarrow \text{H}_2 + 2*$).³⁵ The Tafel slope for the 1 nm-thick a-MoS_x is ~142 mV/dec, suggesting that the Volmer step is dominant due to the exposure of the Ti surface with the island growth of a-MoS_x. However, the Tafel slope decreased to ~41 to 46 mV/dec when the substrate surface was fully covered with a-MoS_x at a thickness of above 3 nm, indicating that the Heyrovsky step was mainly governing the reaction due to the electrocatalytic activity of a-MoS_x. Figure

2c shows the LSV curves of the p-Si photocathodes with a-MoS_x electrocatalytic layers of various thicknesses; these curves are used to assess the effect of the a-MoS_x layer thickness on the PEC performance. The LSV curves were shifted as the a-MoS_x thickness increased up to 3 nm due to the improved electrocatalytic activity of the a-MoS_x layer, as discussed above. For the 3 nm-thick a-MoS_x, an onset potential (V_{on}) of 0.23 V at 1 mA/cm² and an overpotential for the HER at 10 mA/cm² of 0.106 V are achieved, which are the major descriptors of the PEC performance.^{16,17,36,37} The overpotential value is comparable to record values in the literature for c-MoS₂ (0.08 V) and 1T-MoS₂ (0.1 V), as displayed by the black and red dots, respectively, in Figure 2c.^{16,17}

However, increasing the thickness further deteriorated the PEC performance. Therefore, electrochemical impedance spectroscopy (EIS) was used to analyze the a-MoS_x/Si photocathodes to verify the major factors influencing PEC

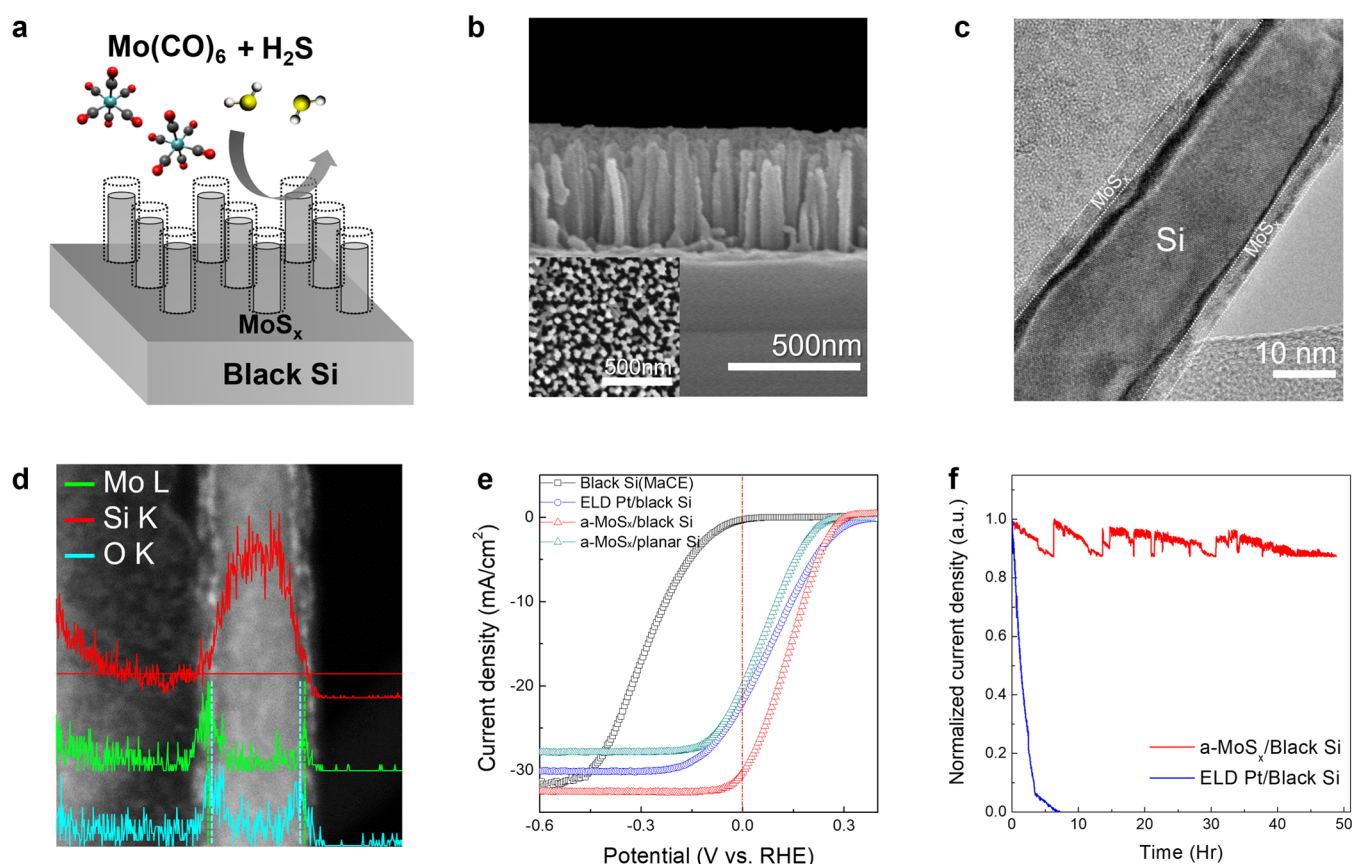


Figure 4. (a) Schematic structure of the black Si with ALD a-MoS_x. (b) Cross-sectional and plan-view (inset) SEM images and (c) HR-TEM images of the ALD a-MoS_x layer on an individual Si nanowire with (d) EDS line scan results suggesting conformal coating of the a-MoS_x layer. (e) LSV response curves of black Si photocathodes with a-MoS_x and ELD Pt. The curve for a-MoS_x/planar Si was also included for comparison. (f) Chronoamperometry measurements for stability testing of a-MoS_x and ELD Pt on the black Si photocathode at 0 V vs RHE. The a-MoS_x/black Si photocathode exhibited better PEC performance and improved stability compared to those of the ELD Pt/black Si photocathode.

performance. Nyquist plots are shown in Figure 2d. The first and second semicircles in the Nyquist plot are associated with the two main resistances for charge transfer from Si to a-MoS_x ($R_{\text{p-Si/cat}}$) and from a-MoS_x to the electrolyte ($R_{\text{cat/Elec}}$), respectively. We evaluated both $R_{\text{p-Si/cat}}$ and $R_{\text{cat/Elec}}$ based on an equivalent circuit consisting of constant-phase elements (the inset of Figure 2d). Figure 2e shows that $R_{\text{cat/Elec}}$, indicated by red circles, rapidly decreased as the nominal thickness of a-MoS_x increased to 3 nm because the surface coverage of the a-MoS_x layer increased to form a continuous film, as discussed above. However, $R_{\text{cat/Elec}}$ gradually increased as the a-MoS_x thickness was increased over 3 nm, which is attributed to the increase in resistance of the a-MoS_x layer. $R_{\text{p-Si/cat}}$, which is indicated by blue squares, monotonically increased as the thickness of the a-MoS_x layer increased. This is because the recombination of photogenerated electrons was suppressed due to the depletion of holes at the Si surface. This phenomenon was induced by the decrease in the Si surface potential built by the a-MoS_x/Si junction, schematically depicted in Figure 2f, which is attributed to the increase in the voltage drop in the a-MoS_x layer as its thickness increased. This was confirmed by calculation results based on the Mott–Schottky plot (Figure S4), where the increased thickness of the a-MoS_x layer leads to a cathodic shift of the flat band voltage (V_{fb}), represented by the x -intercept, suggesting that the Si surface potential decreased. As a result, the total charge transfer resistance ($R_{\text{cat/Elec}} + R_{\text{p-Si/cat}}$) was minimized at 3 nm,

i.e., the optimal thickness of the a-MoS_x layer, thereby resulting in the lowest overpotential and V_{on} required for PEC-HER, as observed in Figure 2c. The cyclic test results in Figure 2g show that the stability of the Si photocathode was significantly improved by the 3 nm-thick a-MoS_x layer. The LSV curve of the bare Si photocathode was considerably shifted as the number of LSV cycles increased; however, the curve of the Si photocathode with the a-MoS_x layer was maintained.

In turn, we compared the LSV responses of Si photocathodes made with the a-MoS_x or c-MoS₂ layer (prepared using RTA) and found that the overpotential of the case with a-MoS_x (0.1 V) is higher than that of the case with c-MoS₂ (−0.17 V), as shown in Figure 3a. The LSV responses of the a-MoS_x and c-MoS₂ layers on Ti foil, as shown in Figure 3b,c, confirm that the better PEC performance of Si photocathodes with the a-MoS_x layer resulted from the improved electrocatalytic activity; the observed Tafel slope of a-MoS_x (41 mV/dec) is much lower than that of c-MoS₂ (113 mV/dec), resulting in the enhanced overpotential (−0.153 and −0.21 V for a-MoS_x and c-MoS₂, respectively). This is due to the dominance of the metallic phase in a-MoS_x, as observed in the XPS results of Figure 1c. The overpotential and Tafel slopes for a-MoS_x and c-MoS_x on conductive substrates were summarized and compared to record reported values for various MoS_x-based HER electrocatalysts, as shown in Figure 3d. Furthermore, the EIS analysis in Figure 3e revealed that the $R_{\text{p-Si/cat}}$ and $R_{\text{cat/Elec}}$ values of a-MoS_x (32.5 and 20 $\Omega\cdot\text{cm}^2$,

Table 1. PEC Performance Parameters from This Work and Previously Reported MoS_x/Si Photocathode Results

no.	photocathode	V_{on} (V vs RHE)	overpotential @ 10 mA/cm ² (V vs RHE)	potential difference ($V_{\text{on}} - V_{\text{overpotential}}$)	J_{sat} (mA/cm ²)	J_{sat} of Si (mA/cm ²)	ref
1	ALD MoS _x /p-Si	0.23	0.106	0.122	27.9	24.7	this work
2	ELD Pt/p-Si	0.21	0.094	0.116	23.9	24.7	this work
3	ALD MoS _x /black Si	0.27	0.2	0.07	32.6	31.8	this work
4	ELD Pt/black Si	0.3	0.14	0.16	29.8	31.8	this work
5	2H MoS ₂ /p-Si	0.17	0.082	0.088	42	40	15
6	1T-MoS ₂ /p-Si	0.25	0.1	0.15	26.7	25	14
7	PEALD MoS ₂ /p-Si	0.23	0.11	0.12	31	27	29
8	chemical MoS ₂ /TiO ₂ /p-SiNW	0.25	0.075	0.175	25		35
9	CVD MoS ₂ /p-SiNW	0.19	0.1	0.09	33		37
10	Pt/p-SiNW	0.33	0.15	0.18	24	26	36

respectively) are much lower than those of c-MoS₂ (68.7 and 32.9 Ω·cm², respectively). This is attributed to the larger surface band bending of the Si photocathode with a-MoS_x, which suppresses the recombination of photogenerated electrons at the Si surface (the interface with a-MoS_x) by depleting the number of holes, as shown in Figure 3f. This effect originates from the higher work function of a-MoS_x than that of c-MoS₂,³⁴ which was confirmed by the ultraviolet photoelectron spectroscopy (UPS) results shown in Figure 3f. The larger surface band bending of the Si photocathode with a-MoS_x is also supported by the Mott–Schottky plot in Figure 3h, showing that the value of V_{fb} for a-MoS_x is higher than that of c-MoS₂. The observed work function of a-MoS_x (4.0 eV) grown using ALD in this work is the lowest value reported so far (see Table SI).³⁸ In addition, the increased open-circuit voltage (V_{oc}), caused by the higher work function of a-MoS_x (Figure 3e), contributed to the decrease in V_{on} and the overpotential.

The ALD a-MoS_x electrocatalyst layer was also employed for nanostructured Si photocathodes (black Si), which have an average light absorbance of ~95% in the broad wavelength region of incident light (see Figure S5). Black Si was fabricated by the metal-assisted chemical etching (MaCE) method,^{39–41} and a 1 nm-thick SiO₂ surface passivation layer was grown using rapid thermal oxidation. The schematic structure of the black Si photocathode is illustrated in Figure 4a. The cross-sectional and plan-view SEM images (Figure 4b) show vertically aligned Si nanowires with an average length of 400 nm (see Figure S6). The HRTEM image (Figure 4c) and EDS line profile (Figure 4d) confirm the conformal deposition of the ALD a-MoS_x layer with an SiO₂ interlayer on individual Si nanowires of black Si.

The LSV response of a-MoS_x/black Si was compared with that of bare black Si and the electroless deposited (ELD) Pt/black Si (Figure 4e). The results from a-MoS_x/planar Si were also included for comparison. The a-MoS_x/black Si exhibited a lower overpotential and saturated photocurrent (J_{sat}) than a-MoS_x/planar Si due to the increase in the light absorbance and the active surface area for the HER, respectively. The overpotential of a-MoS_x/black Si (~0.27 V) was superior to that of ELD Pt/black Si and other previously reported molybdenum sulfide/Si nanostructure photocathodes (see Table 1).^{16,36,37,42–44} The value of J_{sat} is also higher for a-MoS_x/black Si (32.6 mA/cm²) than that of ELD Pt/black Si because there was no reduction of J_{sat} by a-MoS_x deposition

due to its optical transparency, while shadowing loss caused by Pt deposition reduces J_{sat} (29.8 mA/cm²). The wet chemical-based ELD Pt process has difficulty providing a uniform coating on the inside of the nanowires, and thus, coating is mainly done at the tip of the nanowire structures. This lowers both the incident light absorption and the number of active sites with catalysts, which decreased the J_{sat} and slope of the LSV curves. The long-term stabilities of a-MoS_x/black Si and ELD Pt/black Si were compared using chronoamperometry measurements at 0 V, as shown in Figure 4f. Thanks to the conformal deposition of the a-MoS_x layer protecting the surface of black Si against the electrolyte, the a-MoS_x/black Si operated stably for 50 h, while the Pt/black Si photocathode was rapidly degraded over the measurement time.

CONCLUSIONS

We demonstrated the improved PEC performance of a black Si photocathode with an a-MoS_x electrocatalyst layer grown using ALD in an acidic electrolyte. The as-grown MoS_x ($x = 1.7$) exhibited an amorphous nature that was locally composed of an octahedral structure (S-deficient metallic phase) with S vacancies, which promoted high HER electrocatalytic activity. In addition, the smaller work function of a-MoS_x compared to that of c-MoS₂ (4.5 eV) leads to the formation of larger energy band bending at the p-Si surface, which facilitates interface charge transfer and a higher thermodynamic photovoltage. As a result, the kinetic overpotential and onset potential were significantly improved. The a-MoS_x electrocatalyst layer was also applied to a black Si photocathode. Conformal deposition of the a-MoS_x layer was observed on individual Si nanowires in black Si, and an onset potential of 0.27 V and overpotential of 0.2 V were achieved, which are superior to those achieved with an ELD Pt/black Si photocathode. Furthermore, stable, long-term PEC-HER operation for 50 h was ensured. This work provides insights into the application of a versatile a-MoS_x layer for the highly efficient and sustainable operation of black Si photocathodes.

EXPERIMENTAL METHODS

MoS_x Layer Growth via Atomic Layer Deposition. A p-type Si (100) wafer (1–10 Ω cm) and Ti foil were used as substrates for examining the PEC responses and electrocatalytic activity, respectively. A Si wafer was dipped into a dilute HF solution (10 vol %) for 30 s to remove the native oxide. A MoS_x layer was grown using ALD at 178 °C in a 4 in., traveling wave-type reactor using Mo(CO)₆ and

H₂S (5% H₂S/95% N₂) as a metal precursor and a sulfur source, respectively. High-purity N₂ gas (99.999%) was used as a carrier gas and a purging gas. A Mo(CO)₆ precursor was heated to 35 °C in a bubbler-type canister. An ALD cycle consists of Mo precursor feeding, N₂ purging, H₂S feeding, and N₂ purging. The thickness of the MoS_x film was controlled by adjusting the number of ALD cycles and monitored using spectroscopic ellipsometry (MG-1000, Nano-View). For the crystalline c(2H)-MoS₂ device, RTA was immediately followed at 800 °C for 90 s in an H₂S atmosphere (100 torr) for crystallization of the ALD a-MoS_x layer.

Black Si Photocathode Fabrication. A black Si substrate was fabricated by the MaCE method, which utilizes nanoscale etching of the Si surface where metal nanoparticles are deposited using an etchant. After a dilute HF solution (10 vol %) was used to remove the native oxide, the Si substrate was immersed in a mixture solution of diluted HF (50 vol %, 4.8 M) and AgNO₃ (0.005 M) to coat the Ag nanoparticles. Subsequently, the Ag nanoparticle-coated Si substrate was etched by immersing it in a mixture solution of H₂O₂ (0.5 M) and HF (4.8 M), followed by dipping it in a diluted HNO₃ solution to remove the residual Ag nanoparticles. A 1 nm-thick SiO₂ surface passivation layer was grown using rapid thermal oxidation at 800 °C for 10 s under O₂ ambient conditions with 15 torr. Pt deposition was conducted using ELD with 0.4 M HF + 1 mM K₂PtCl₆ (Sigma-Aldrich, 99.9%). Deposition times were adjusted from 3 to 40 min and optimized at 3 min for the best PEC performance, which was chosen as a reference device (Figure 4d). We fabricated more than five samples per batch, and we also fabricated them several times to secure reproducibility.

Material Characterization. Chemical binding states of the MoS_x films were examined by XPS (Thetaprobe, Thermo Scientific) using Al-K α as the X-ray source. Binding energies were calibrated using C–C binding energy in the C 1s spectrum (284.5 eV) of the adventitious carbon as an internal standard. UPS (Thetaprobe, Thermo Scientific) analysis was conducted using a UV source of He I (21.2 eV). Raman spectroscopy (582 nm) was used to examine the crystallinity of the a-MoS_x and c-MoS₂ layers. The light reflectance of the black Si substrate was measured using UV/Vis/NIR spectrophotometry (Lambda 750, PerkinElmer). The microstructures of the a-MoS_x layer grown on the planar Si and black Si were observed through HR-TEM equipped with a field emission gun (JEM-2100F, JEOL). The morphology of black Si was characterized via FE-SEM (S-4800, Hitachi).

Electrical Measurements. The PEC performance of the Si photocathodes was evaluated in a 0.5 M H₂SO₄ aqueous solution using a solar simulator (PEC-L11, Pectell Tech.) under air-mass (AM) 1.5G (100 mW/cm²) illumination with a three-electrode configuration comprising a working electrode, an Ag/AgCl reference electrode, and a Pt mesh counter electrode. The photocurrent spectra were calibrated using a Si photodiode standard cell (PV Measurement, Inc.). All of the measured potentials vs Ag/AgCl were converted into RHE potentials with a 0.5 M H₂SO₄ aqueous electrolyte condition. EIS was obtained at –0.02 V vs RHE with a measurement frequency range of 1 Hz–200 kHz. The resistance at each interface was evaluated using a semicircle in the Nyquist plot. Capacitance–voltage measurements for the Mott–Schottky (M–S) plot were performed at a frequency of 10 kHz. All the data were statistically processed after several measurements to confirm the reproducibility.

■ ASSOCIATED CONTENT

■ Supporting Information

The Supporting Information is available free of charge at <https://pubs.acs.org/doi/10.1021/acsami.1c22273>.

Growth rate of ALD a-MoS_x films; XPS core-level spectra; AFM images; Mott–Schottky plots; and UV–Vis reflectance spectra of black Si (PDF)

■ AUTHOR INFORMATION

Corresponding Authors

Yo-Sep Min – Department of Chemical Engineering, Konkuk University, Seoul 05029, Korea; orcid.org/0000-0002-2340-3633; Email: ysmin@konkuk.ac.kr

Jung-Ho Lee – Department of Materials Science and Chemical Engineering, Hanyang University, Ansan 15588, Korea; orcid.org/0000-0002-6731-3111; Email: jungho@hanyang.ac.kr

Tae Joo Park – Department of Materials Science and Chemical Engineering, Hanyang University, Ansan 15588, Korea; Department of Advanced Materials Engineering, Hanyang University, Ansan 15588, Korea; orcid.org/0000-0003-4641-2425; Email: tjp@hanyang.ac.kr

Authors

Dae Woong Kim – Department of Materials Science and Chemical Engineering, Hanyang University, Ansan 15588, Korea; Advanced Materials Research Team, Hyundai Motor Company, Uiwang 16082, Korea; orcid.org/0000-0003-1906-244X

Jin-Young Jung – Department of Materials Science and Chemical Engineering, Hanyang University, Ansan 15588, Korea

Dae Hyun Kim – Department of Advanced Materials Engineering, Hanyang University, Ansan 15588, Korea

Jin-Young Yu – Department of Materials Science and Chemical Engineering, Hanyang University, Ansan 15588, Korea

Jae Hyuck Jang – Center for Research Equipment, Korea Basic Science Institute, Daejeon 169-148, Korea; orcid.org/0000-0002-9133-3286

Hyun Soo Jin – Department of Materials Science and Chemical Engineering, Hanyang University, Ansan 15588, Korea

Tae Jun Seok – Department of Materials Science and Chemical Engineering, Hanyang University, Ansan 15588, Korea

Complete contact information is available at:

<https://pubs.acs.org/doi/10.1021/acsami.1c22273>

Author Contributions

#D.W.K. and J.-Y.J. contributed equally.

Notes

The authors declare no competing financial interest.

■ ACKNOWLEDGMENTS

This work was supported by the Ministry of Trade, Industry and Energy (MOTIE, 20010275), Basic Science Research Program through the National Research Foundation of Korea, which is funded by the Ministry of Education (NRF: 2021R1F1A1059930), and the Korea Basic Science Institute (KBSI) research (Grant No. C180400).

■ REFERENCES

- (1) Grätzel, M. Photoelectrochemical cells. *Nature* **2001**, 414, 338–344.
- (2) Peng, K.-Q.; Wang, X.; Li, L.; Hu, Y.; Lee, S.-T. Silicon Nanowires for Advanced Energy Conversion and Storage. *Nano Today* **2013**, 8, 75–97.
- (3) Peng, W.; Rupich, S. M.; Shafiq, N.; Gartstein, Y. N.; Malko, A. V.; Chabal, Y. J. Silicon Surface Modification and Characterization for

Emergent Photovoltaic Applications Based on Energy Transfer. *Chem. Rev.* **2015**, *115*, 12764–12796.

(4) Oh, J.; Deutsch, T. G.; Yuan, H.-C.; Branz, H. M. Nanoporous Black Silicon Photocathode for H₂ Production by Photoelectrochemical Water Splitting. *Energy Environ. Sci.* **2011**, *4*, 1690–1694.

(5) Oh, I.; Kye, J.; Hwang, S. Enhanced Photoelectrochemical Hydrogen Production from Silicon Nanowire Array Photocathode. *Nano Lett.* **2012**, *12*, 298–302.

(6) Jung, J.-Y.; Choi, M. J.; Zhou, K.; Li, X.; Jee, S.-W.; Um, H.-D.; Park, M.-J.; Park, K.-T.; Bang, J. H.; Lee, J.-H. Photoelectrochemical Water Splitting Employing a Tapered Silicon Nanohole Array. *J. Mater. Chem. A* **2014**, *2*, 833–842.

(7) Wang, Y.-C.; Liu, X.-Y.; Wang, X.-X.; Cao, M.-S. Metal-organic frameworks based photocatalysts: Architecture strategies for efficient solar energy conversion. *Chem. Eng. J.* **2021**, *419*, No. 129459.

(8) Hu, S.; Shaner, M. R.; Beardslee, J. A.; Lichterman, M.; Brunswig, B. S.; Lewis, N. S. Amorphous TiO₂ Coatings Stabilize Si, GaAs, and GaP Photoanodes for Efficient Water Oxidation. *Science* **2014**, *344*, 1005–1009.

(9) Yang, J.; Walczak, K.; Anzenberg, E.; Toma, F. M.; Yuan, G.; Beeman, J.; Schwartzberg, A.; Lin, Y.; Hettick, M.; Javey, A.; et al. Efficient and Sustained Photoelectrochemical Water Oxidation by Cobalt Oxide/Silicon Photoanodes with Nanotextured Interfaces. *J. Am. Chem. Soc.* **2014**, *136*, 6191–6194.

(10) Walter, M. G.; Warren, E. L.; McKone, J. R.; Boettcher, S. W.; Mi, Q.; Santori, E. A.; Lewis, N. S. Solar Water Splitting Cells. *Chem. Rev.* **2010**, *110*, 6446–6473.

(11) Dai, P.; Xie, J.; Mayer, M. T.; Yang, X.; Zhan, J.; Wang, D. Solar Hydrogen Generation by Silicon Nanowires Modified with Platinum Nanoparticle Catalysts by Atomic Layer Deposition. *Angew. Chem.* **2013**, *125*, 11325–11329.

(12) Voiry, D.; Salehi, M.; Silva, R.; Fujita, T.; Chen, M.; Asefa, T.; Shenoy, V. B.; Eda, G.; Chhowalla, M. Conducting MoS₂ Nanosheets as Catalysts for Hydrogen Evolution Reaction. *Nano Lett.* **2013**, *13*, 6222–6227.

(13) Cheng, L.; Huang, W.; Gong, Q.; Liu, C.; Liu, Z.; Li, Y.; Dai, H. Ultrathin WS₂ Nanoflakes as a High-performance Electrocatalyst for the Hydrogen Evolution Reaction. *Angew. Chem., Int. Ed.* **2014**, *53*, 7860–7863.

(14) Dominey, R. N.; Lewis, N. S.; Bruce, J. A.; Bookbinder, D. C.; Wrighton, M. S. Improvement of Photoelectrochemical Hydrogen Generation by Surface Modification of p-type Silicon Semiconductor Photocathodes. *J. Am. Chem. Soc.* **1982**, *104*, 467–482.

(15) Jaramillo, T. F.; Jørgensen, K. P.; Bonde, J.; Nielsen, J. H.; Horch, S.; Chorkendorff, I. Identification of Active Edge Sites for Electrochemical H₂ Evolution from MoS₂ Nanocatalysts. *Science* **2007**, *317*, 100–102.

(16) Ding, Q.; Meng, F.; English, C. R.; Cabán-Acevedo, M.; Shearer, M. J.; Liang, D.; Daniel, A. S.; Hamers, R. J.; Jin, S. Efficient Photoelectrochemical Hydrogen Generation Using Heterostructures of Si and Chemically Exfoliated Metallic MoS₂. *J. Am. Chem. Soc.* **2014**, *136*, 8504–8507.

(17) Kwon, K. C.; Choi, S.; Hong, K.; Moon, C. W.; Shim, Y.-S.; Kim, D. H.; Kim, T.; Sohn, W.; Jeon, J.-M.; Lee, C.-H.; Nam, K. T.; Han, S.; Kim, S. Y.; Jang, H. W. Wafer-scale Transferable Molybdenum Disulfide Thin-film Catalysts for Photoelectrochemical Hydrogen Production. *Energy Environ. Sci.* **2016**, *9*, 2240–2248.

(18) Siavash Moakhar, R.; Hosseini-Hosseinabad, S. M.; Masudypanah, S.; Seza, A.; Jalali, M.; Fallah-Arani, H.; Dabir, F.; Gholipour, S.; Abdi, Y.; Bagheri-Hariri, M.; et al. Photoelectrochemical Water-Splitting Using CuO-Based Electrodes for Hydrogen Production: A Review. *Adv. Mater.* **2021**, *33*, No. 2007285.

(19) Merki, D.; Fierro, S.; Vrubel, H.; Hu, X. Amorphous Molybdenum Sulfide Films as Catalysts for Electrochemical Hydrogen Production in Water. *Chem. Sci.* **2011**, *2*, 1262–1267.

(20) Lu, A.-Y.; Xiulin, Y.; Chien-Chih, T.; Shixiong, M.; Shi-Hsin, L.; Chang-Lung, H.; Henan, L.; Hicham, I.; Jer-Lai, K.; Kuo-Wei, H.; Lain-Jong, L. High-Sulfur-Vacancy Amorphous Molybdenum Sulfide

as a High Current Electrocatalyst in Hydrogen Evolution. *Small* **2016**, *12*, 5530–5537.

(21) Vrubel, H.; Hu, X. Growth and Activation of an Amorphous Molybdenum Sulfide Hydrogen Evolving Catalyst. *ACS Catal.* **2013**, *3*, 2002–2011.

(22) Zhou, J.; Dai, S.; Dong, W.; Su, X.; Fang, L.; Zheng, F.; Wang, X.; Shen, M. Efficient and Stable MoS₂ Catalyst Integrated on Si Photocathodes by Photoreduction and Post-annealing for Water Splitting. *Appl. Phys. Lett.* **2016**, *108*, No. 213905.

(23) Li, H.; Tsai, C.; Koh, A. L.; Cai, L.; Contryman, A. W.; Fragapane, A. H.; Zhao, J.; Han, H. S.; Manoharan, H. C.; Abild-Pedersen, F.; Nørskov, J. K.; Zheng, X. Corrigendum: Activating and Optimizing MoS₂ Basal Planes for Hydrogen Evolution Through the Formation of Strained Sulphur Vacancies. *Nat. Mater.* **2016**, *15*, 364.

(24) Andoshe, D. M.; Jin, G.; Lee, C. S.; Kim, C.; Kwon, K. C.; Choi, S.; Sohn, W.; Moon, C. W.; Lee, S. H.; Suh, J. M.; Kang, S.; Park, J.; Heo, H.; Kim, J. K.; Han, S.; Jo, M. H.; Jang, H. W. Directly Assembled 3D Molybdenum Disulfide on Silicon Wafer for Efficient Photoelectrochemical Water Reduction. *Adv. Sustainable Syst.* **2018**, *2*, No. 1700142.

(25) Islam, M. A.; Church, J.; Han, C.; Chung, H.-S.; Ji, E.; Kim, J. H.; Choudhary, N.; Lee, G.-H.; Lee, W. H.; Jung, Y. Noble Metal-coated MoS₂ Nanofilms with Vertically-aligned 2D Layers for Visible Light-driven Photocatalytic Degradation of Emerging Water Contaminants. *Sci. Rep.* **2017**, *7*, No. 14944.

(26) Lukowski, M. A.; Daniel, A. S.; Meng, F.; Forticaux, A.; Li, L.; Jin, S. Enhanced Hydrogen Evolution Catalysis from Chemically Exfoliated Metallic MoS₂ Nanosheets. *J. Am. Chem. Soc.* **2013**, *135*, 10274–10277.

(27) Pyeon, J. J.; Kim, S. H.; Jeong, D. S.; Baek, S.-H.; Kang, C.-Y.; Kim, J.-S.; Kim, S. K. Wafer-scale Growth of MoS₂ Thin Films by Atomic Layer Deposition. *Nanoscale* **2016**, *8*, 10792–10798.

(28) Guo, X.; Hou, Y.; Ren, R.; Chen, J. Temperature-dependent Crystallization of MoS₂ Nanoflakes on Graphene Nanosheets for Electrocatalysis. *Nanoscale Res. Lett.* **2017**, *12*, No. 479.

(29) Tan, L. K.; Liu, B.; Teng, J. H.; Guo, S.; Low, H. Y.; Loh, K. P. Atomic Layer Deposition of a MoS₂ Film. *Nanoscale* **2014**, *6*, 10584–10588.

(30) Kappera, R.; Voiry, D.; Yalcin, S. E.; Jen, W.; Acerce, M.; Torrel, S.; Branch, B.; Lei, S.; Chen, W.; Najmaei, S.; Lou, J.; Ajayan, P. M.; Gupta, G.; Mohite, A. D.; Chhowalla, M. Metallic 1T Phase Source/Drain Electrodes for Field Effect Transistors from Chemical Vapor Deposited MoS₂. *APL Mater.* **2014**, *2*, No. 092516.

(31) Jin, Z.; Shin, S.; Kwon, D. H.; Han, S.-J.; Min, Y.-S. Novel Chemical Route for Atomic Layer Deposition of MoS₂ Thin Film on SiO₂/Si Substrate. *Nanoscale* **2014**, *6*, 14453–14458.

(32) Acerce, M.; Voiry, D.; Chhowalla, M. Metallic 1T Phase MoS₂ Nanosheets as Supercapacitor Electrode Materials. *Nat. Nanotechnol.* **2015**, *10*, 313.

(33) Eda, G.; Yamaguchi, H.; Voiry, D.; Fujita, T.; Chen, M.; Chhowalla, M. Photoluminescence from Chemically Exfoliated MoS₂. *Nano Lett.* **2011**, *11*, 5111–5116.

(34) Shin, S.; Jin, Z.; Ham, S.-Y.; Lee, S.; Shin, D.-S.; Min, Y.-S. Effect of Oxygen Incorporation in Amorphous Molybdenum Sulfide on Electrochemical Hydrogen Evolution. *Appl. Surf. Sci.* **2019**, *487*, 981–989.

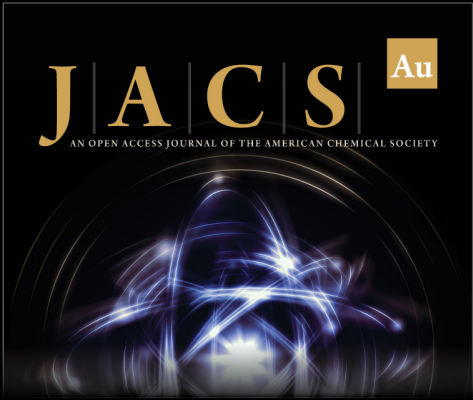
(35) Bockris, J. O. M.; Potter, E. C. The Mechanism of the Cathodic Hydrogen Evolution Reaction. *J. Electrochem. Soc.* **1952**, *99*, 169–186.

(36) Oh, S.; Kim, J. B.; Song, J. T.; Oh, J.; Kim, S.-H. Atomic Layer Deposited Molybdenum Disulfide on Si Photocathodes for Highly Efficient Photoelectrochemical Water Reduction Reaction. *J. Mater. Chem. A* **2017**, *5*, 3304–3310.


(37) Hou, Y.; Zhu, Z.; Xu, Y.; Guo, F.; Zhang, J.; Wang, X. Efficient Photoelectrochemical Hydrogen Production Over p-Si Nanowire Arrays Coupled with Molybdenum–sulfur Clusters. *Int. J. Hydrogen Energy* **2017**, *42*, 2832–2838.


(38) Ye, J.; Li, X.; Zhao, J.; Mei, X.; Li, Q. A Facile Way to Fabricate High-performance Solution-processed n-MoS₂/p-MoS₂ Bilayer Photodetectors. *Nanoscale Res. Lett.* **2015**, *10*, No. 454.

- (39) Kim, D. W.; Song, J.-W.; Jin, H. S.; Yoo, B.; Lee, J.-H.; Park, T. J. Sulfur-Enhanced Field-Effect Passivation using (NH₄)₂S Surface Treatment for Black Si Solar Cells. *ACS Appl. Mater. Interfaces* **2019**, *11*, 25140–25146.
- (40) Song, J.-W.; Nam, Y.-H.; Park, M.-J.; Shin, S.-M.; Wehrspohn, R. B.; Lee, J.-H. Hydroxyl Functionalization Improves the Surface Passivation of Nanostructured Silicon Solar Cells Degraded by Epitaxial Regrowth. *RSC Adv.* **2015**, *5*, 39177–39181.
- (41) Kim, D. W.; Song, J.-W.; Park, Y. M.; Lee, J.-H.; Park, T. J. Novel Field-effect Passivation for Nanostructured Si Solar Cells Using Interfacial Sulfur Incorporation. *Prog. Photovolt.: Res. Appl.* **2017**, *25*, 376–383.
- (42) Zhang, L.; Liu, C.; Wong, A. B.; Resasco, J.; Yang, P. MoS₂-wrapped Silicon Nanowires for Photoelectrochemical Water Reduction. *Nano Res.* **2015**, *8*, 281–287.
- (43) Jung, J.-Y.; Park, M.-J.; Li, X.; Kim, J.-H.; Wehrspohn, R. B.; Lee, J.-H. High Performance H₂ Evolution Realized in 20 μm-thin Silicon Nanostructured Photocathodes. *J. Mater. Chem. A* **2015**, *3*, 9456–9460.
- (44) Paulraj, G.; Venkatesh, P. S.; Dharmaraj, P.; Gopalakrishnan, S.; Jeganathan, K. Stable and Highly Efficient MoS₂/SiNWs Hybrid Heterostructure for Photoelectrocatalytic Hydrogen Evolution Reaction. *Int. J. Hydrogen Energy* **2020**, *45*, 1793–1801.




JACS Au
AN OPEN ACCESS JOURNAL OF THE AMERICAN CHEMICAL SOCIETY

 Editor-in-Chief
Prof. Christopher W. Jones
Georgia Institute of Technology, USA

Open for Submissions 

pubs.acs.org/jacsau

 **ACS Publications**
Most Trusted. Most Cited. Most Read.

Supporting Information

Black Si Photocathode with a Conformal and Amorphous MoS_x Catalytic Layer Grown Using Atomic Layer Deposition for Photoelectrochemical Hydrogen Evolution

Dae Woong Kim,^{1, 5, ‡} Jin-Young Jung,^{1, ‡} Dae Hyun Kim,² Jin-Young Yu,¹ Jae Hyuck Jang,

*³ Hyun Soo Jin¹, Tae Jun Seok¹, Yo-Sep Min,^{4, *} Jung-Ho Lee,^{1, *} and Tae Joo Park^{1,2, *}*

¹ Department of Materials Science and Chemical Engineering, Hanyang University, Ansan 15588, Korea

² Department of Advanced Materials Engineering, Hanyang University, Ansan 15588, Korea

³ Center for Research Equipment, Korea Basic Science Institute, Daejeon 169-148, Korea

⁴ Department of Chemical Engineering, Konkuk University, Seoul 05029, Korea

⁵ Advanced Materials Research Team, Hyundai Motor Company, Uiwang 16082, Korea

* Corresponding authors

‡ These authors equally contributed to the presented work

Email: tjp@hanyang.ac.kr, jungho@hanyang.ac.kr, ysmin@konkuk.ac.kr

Supporting Information contains:

- Figs. S1: Thickness of MoS_x films measured by Ellipsometry
- Figs. S2: XPS core level spectra of the ALD a-MoS_x film
- Figs. S3: AFM images and RMS roughness of ALD a-MoS_x films
- Figs. S4: Mott–Schottky plots ($1/C^2$ vs. V) of a-MoS_x films
- Figs. S5: UV-Vis reflectance spectra of the semiconductor substrates
- Table S1: Electronic properties of reported molybdenum sulfides

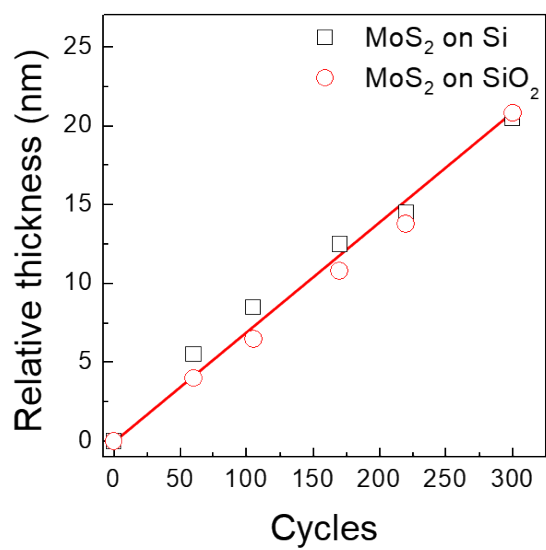


Figure S1. Thickness of MoS_x films on Si and SiO₂ substrates as a function of the number of ALD cycles.

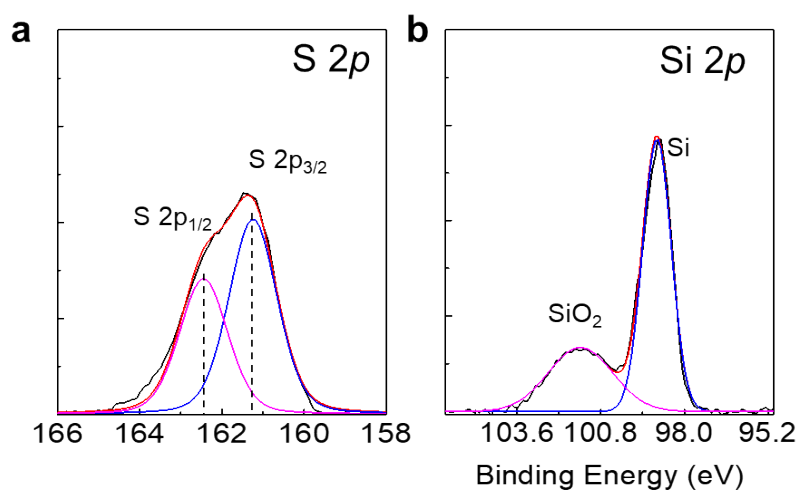


Figure S2. (a) S 2p and (b) Si 2p core level spectra of the ALD a-MoS_x film on an Si substrate.

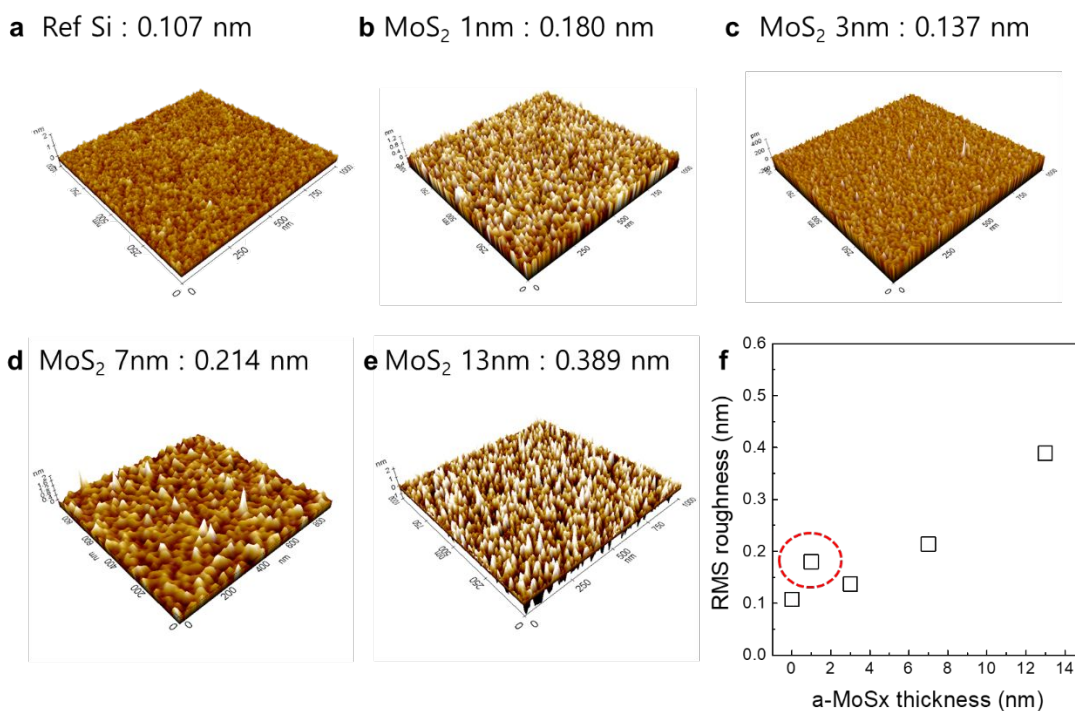


Figure S3. AFM images of ALD a-MoS_x films with various thicknesses on Si substrates and the corresponding RMS roughness as a function of the a-MoS_x film thickness.

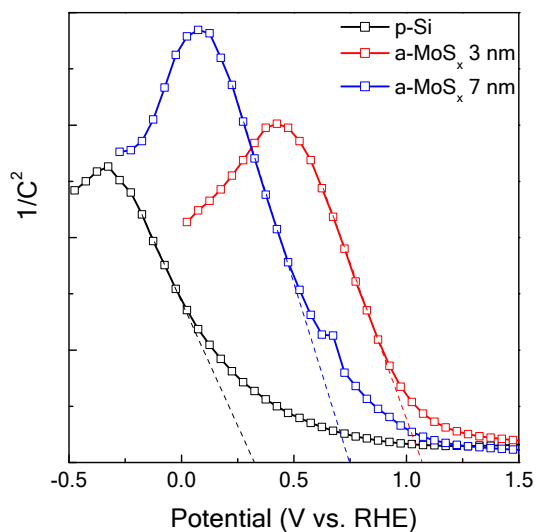


Figure S4. Mott–Schottky plots ($1/C^2$ vs. V) of a-MoS_x films with various thicknesses on Si substrates for estimating V_{fb} .

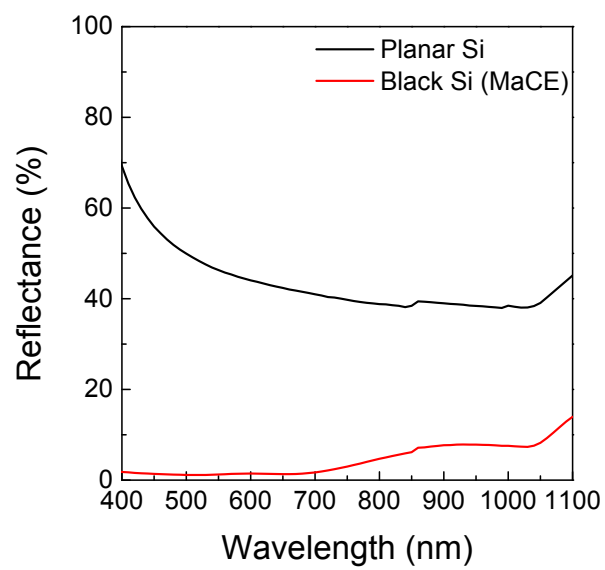


Figure S5. UV-Vis reflectance spectra of the planar Si wafer and black Si substrates.

Table S1. Electronic properties of molybdenum sulfides from this work and from the literature.

	Growth method	Crystal structure	Workfunc. Ø (eV)	E_g (eV)	Ref.
1	Thermolysis	c-MoS ₂	4.5	1.6	1, 2
2	Mo sulfurization	c-MoS ₂	4.57	1.59	3
3	Exfoliation	c-MoS ₂	4.3	2.3	4
4	DC magnetron sputtering	c-MoS ₂	5.53	1.48	5
5	Exfoliation	c-MoS ₂	4.63	1.8	6
6	Pulsed laser deposition	a-MoS ₂	5.16	1.37	7
7	ALD	a-MoS ₂	4.0	2	This work

1. *Energy Environ. Sci.*, 2016, 9, 2240
2. *J. Mater. Chem. A*, 2017, 5, 15534
3. *Sci Rep.* 2017; 7: 14944.
4. *Nanoscale Research Letters*, 2015, **10**:454
5. *Nanoscale Research Letters*, 2017, **12**:567
6. *Adv. Mater.* 2015, 27, 1175–1181
7. *ACS Appl. Mater. Interfaces* 2017, 9, 18362–18368